ACS Catalysis

Research Article

pubs.acs.org/acscatalysis

Chemical, Structural, and Morphological Changes of a MoVTeNb Catalyst during Oxidative Dehydrogenation of Ethane

Jaime S. Valente,*[,†] Héctor Armendáriz-Herrera,*[,†] Roberto Quintana-Solórzano,[†] Paz del Ángel,[†] Noel Nava,[†] Amada Massó,[‡] and José M. López Nieto[‡]

[†]Instituto Mexicano del Petróleo, Eje Central No. 152, México, D.F. 07730, México

[‡]Instituto de Tecnología Química, UPV-CSIC, Campus de la Universidad Politécnica de Valencia, Av. Los Naranjos s/n, 46022 Valencia, Spain

ABSTRACT: MoVTeNb mixed oxide, a highly active and selective catalyst for the oxidative dehydrogenation of ethane to produce ethylene, exhibits the so-called M1 and M2 crystalline phases. The thermal stability of the MoVTeNb catalytic system was assessed under varying reaction conditions; to this end, the catalyst was exposed to several reaction temperatures spanning from 440 to 550 °C. Both the pristine and spent materials were analyzed by several characterization techniques. The catalyst was stable below 500 °C; a reaction temperature of ≥500 °C brings about the removal of tellurium from the intercalated framework channels of the M1 crystalline phase. Rietveld refinement of X-ray diffraction patterns and microscopy results showed that the tellurium loss causes the progressive partial destruction of the M1 phase, thus decreasing the number of active sites and forming a MoO_2 crystalline phase, which is inactive for this reaction. Raman spectroscopy confirmed the MoO_2 phase development as a function of reaction temperature. From high-resolution transmission electron microscopy and energy-dispersive X-ray spectroscopy analyses it was noticed that tellurium departure occurs preferentially from the end sides of the needlelike M1 crystals, across the [001] plane. Detailed analysis of a solid deposited at the reactor outlet showrf that it consisted mainly of metallic tellurium, suggesting that the tellurium detachment occurs via reduction of Te^{4+} to Te^0 due to a combination of reaction temperature and feed composition. Thus, in order to sustain the catalytic performance exhibited by MoVTeNb mixed oxide, hot spots along the reactor bed should be avoided or controlled, maintaining the catalytic bed temperature below 500 °C.

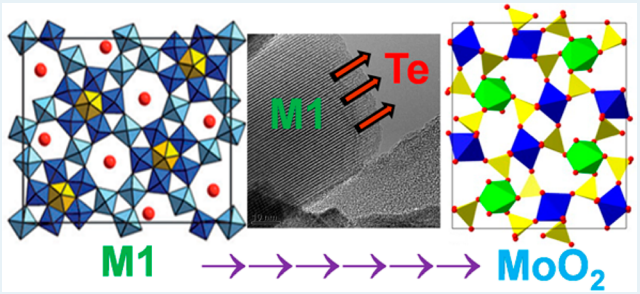

KEYWORDS: *oxidative dehydrogenation, ethane, ethylene, thermal stability, M1 and M2 phases, MoO_2*

1. INTRODUCTION

Ethylene is the keystone of the petrochemical industry, being the main building block as well as the major feedstock for polymer production. Currently, most of the ethylene commercialized in the world is obtained by pyrolysis (steam cracking) of different hydrocarbon streams; also, fluid catalytic cracking (FCC) and catalytic dehydrogenation of ethane contribute marginally. The ethylene market is expected to increase in the coming years, since ethylene's demand is related to population growth.[1] Steam cracking is carried out at high temperatures, ranging from 800 to 900 °C; hence, the energy consumption of the process is considerable.[2] Apart from consuming a large amount of energy and requiring a special metallurgy for the furnace internal components, high-temperature steam cracking operation increases the occurrence of side reactions, decreasing the global selectivity for ethylene and resulting in the formation of a large diversity of byproducts such as acetylene, hydrogen, methane, etc., which are difficult to separate from the main reactor effluent, requiring complex downstream separation processes.[3,4]

On the other hand, an unfavored thermodynamic equilibrium restricts the yield of catalytic dehydrogenation of ethane at moderate temperatures (<600 °C).[5] Even though catalysts are used to increase ethane conversion and ethylene selectivity, they are very susceptible to coke deactivation.[6] Restoring the catalyst's activity is possible but requires a special engineering configuration, which appreciably augments the operation costs.

Attention has now focused on other routes to produce ethylene, paying particular attention to processes that may overcome the disadvantages characterizing steam cracking and catalytic dehydrogenation processes.

For several years, oxidative dehydrogenation of ethane ($ODH\text{-}C_2$) has been studied as a plausible technological alternative for ethylene production. $ODH\text{-}C_2$ is performed via a heterogeneously catalyzed process in which ethane reacts with an oxidant species.[4,5,7] Several advantages are detected when $ODH\text{-}C_2$ is contrasted with direct dehydrogenation: (i) no thermodynamic limitations exist; (ii) reactions are exothermic, thus avoiding the need to supply heat by external means; (iii)

Received: February 3, 2014
Revised: March 17, 2014
Published: March 18, 2014

the products are limited in number and can easily be tracked and handled; and (iv) no coke formation occurs.[8]

Producing ethylene via ODH-C_2 at a commercial scale is still a challenge. One of the main issues to be tackled is, undoubtedly, having a catalyst with adequate properties to produce ethylene selectively and minimize CO_x formation. It has in fact been reported that in an economically attractive industrial scenario for ODH-C_2, the ethylene selectivity should be higher than 90% with ethane conversion ranging from 60 to 80% at temperatures below 500 °C.[2,3,9]

High selectivity for ethylene is one of the most important features of a suitable catalyst, not only for economic feasibility but also because the combustion reactions responsible for the formation of CO and CO_2 are ca. 8 and 13 times more exothermic, respectively, than ethylene production from ethane.[9] This would represent an important issue for operational reactor control because of the hot points generated by the aforementioned combustion reactions.

In this context, a large variety of catalytic systems have been reported in the literature. To date, one of the most outstanding catalysts for ODH-C_2 to give ethylene is a multicomponent catalyst based on MoTeVNb mixed oxides, which has been described and studied by several research groups.[9−16] Certainly, the catalyst must exhibit a multifunctional assortment of properties, since the catalytic performance depends on them. Thus, the crystalline phases play a crucial role in creating and controlling the catalytic centers required.

These MoTeVNb materials consist of mixed oxides mainly composed of the M1 and M2 crystalline phases as well as minor amounts of other phases such as Mo_5O_{14}-type structures or binary MoV and MoTe oxides. M2 is a hexagonal phase with space group *P6mm*, and this phase has been reported to be practically inactive in the ODH-C_2 reaction. The orthorhombic M1 phase, space group *Pba*2 (No. 32) is built from center-occupied pentagonal rings that are linked together by corner-sharing MO_6 octahedrons (M = Mo, V), which are assembled in the [001] plane to form characteristic hexagonal and heptagonal rings hosting Te−O units. Niobium is preferentially located in a pentagonal bipyramidal environment. However, because of a certain chemical flexibility of the phase, octahedral positions may also be occupied by Nb in M1 with higher Nb content. A bronzelike channel structure is thus created by stacking of layers of the polyhedrons in the [001] direction, resulting in a needlelike crystal morphology in which the [001] planes are arranged perpendicular to the length axis of the needle. It has been suggested that terminating [001] planes of the M1 phase contain the most active and selective surface sites for ODH-C_2.[10−24]

This assumption has encouraged worldwide research on the crystalline structures and physicochemical properties of the M1 phase by means of several characterization techniques.[13,23−33] In this sense, López Nieto and co-workers have reported an important tellurium loss during thermal treatment of the catalyst, which is commonly performed at 600 °C under nitrogen.[34] Indeed, the Mo/Te ratio increases when the niobium oxalate content is increased because oxalate anions act as a reducing agent, which enhances the degree of reduction of tellurium cations. This renders the Te unstable and easy to remove from the crystalline structures, as metallic tellurium has a low melting point (ca. 450 °C).

Notwithstanding the inconveniences that arise from the presence of tellurium, it seems to be a key element in most of the highly efficient catalytic systems reported to date for ODH-C_2 to give ethylene (i.e., MoVTeNbO catalysts). Consequently, the relatively high susceptibility of tellurium to reducing atmospheres, together with the large amount of metal that is lost during the thermal activation stages, appears to be a restriction on scale-up of this catalyst to industrial levels. This problem would be always latent in industrial practice since, during operation, the reaction mixture would consist of ethane diluted in nitrogen, a reductive mixture that in the presence of hot spots would favor the reduction and further loss of tellurium, with the consequent gradual decay in the catalytic properties of the solid. However, few reports are available about the thermal stability of MoVTeNb catalyst when it is exposed to severe operating conditions.

Therefore, this work is focused on studying the chemical, structural, and morphological changes occurring over a MoVTeNb catalyst when it is exposed to several reaction temperatures (440, 480, 500, and 550 °C) and their impact on the corresponding catalytic properties, in order to set parameters for maintaining the catalytic performance exhibited by these materials in ODH-C_2. To this end, catalytic tests were carried out in a lab-scale reactor, after which the spent materials were examined using different characterization techniques. The effect of changes on the catalytic properties of the solid was also assessed by performing the ODH-C_2 reaction once more over the spent materials.

2. EXPERIMENTAL SECTION

2.1. Preparation of Catalysts. MoVTeNb mixed oxide with a nominal Mo/V/Te/Nb atomic ratio of 1/0.24/0.24/0.18 was prepared by the slurry method reported elsewhere,[27] which comprises the following steps. First, an aqueous solution containing ammonium heptamolybdate tetrahydrate (Merck, 99%), telluric acid (Aldrich, 98%), and ammonium metavanadate (Sigma-Aldrich, 99.5%) was prepared under continuous stirring at 80 °C (solution A); in parallel, an aqueous solution containing niobium oxalate (ABCR Laboratories, 99%) and oxalic acid (Aldrich, 98%) was also prepared at 80 °C (solution B). Next, solution B was slowly added to solution A under vigorous continuous stirring. The resulting slurry was cooled to room temperature, and then the pH was adjusted to 2.5 using 1 M nitric acid solution. The slurry was rotavaporated at 50 °C and 27 kPa, and the resulting solid was dried overnight at 100 °C and finally thermally treated at 600 °C for 2 h under a flow of nitrogen. The material obtained was labeled as MoVTeNb-F, where "F" stands for "fresh" (or pristine) material.

The pristine catalyst (MoVTeNb-F) was subjected to a series of catalytic tests spanning temperatures from 440 to 550 °C. Samples resulting from such tests, denoted as spent ("S") catalysts, were recovered for characterization. The spent catalysts were coded as MoVTeNb-S440, MoVTeNb-S500, and MoVTeNb-S550, where the number represents the reaction temperature in degrees Celsius used in the test.

2.2. Catalytic Testing. The catalytic experiments were performed in a semiautomated lab-scale setup equipped with a 10 mm internal diameter/40 mm length fixed-bed quartz tubular reactor that was operated isothermally at atmospheric pressure in the integral regime. All of the tests were performed by feeding the reactor with a mixture of ethane (C_2) and oxygen (O_2) as well as nitrogen (N_2) as a diluent. N_2 was also employed as an internal standard. The purities of the ethane, oxygen, and nitrogen utilized in the experiments were 99.7, 99.996, and 99.999 vol %, respectively. The reactor effluent was

dx.doi.org/10.1021/cs500143j | ACS Catal. 2014, 4, 1292−1301

analyzed periodically online by gas chromatography (GC); the detailed setup is reported in ref 9.

The amount of catalyst was 0.6 g (150 μm average size), and the reactor feed was a $C_2/O_2/N_2$ mixture with a molar ratio of 9/7/84. The reaction temperature ranged from 440 to 550 °C, and the space time (W/F°_{ethane}, where W is the mass of catalyst and F°_{ethane} is the molar flow rate of ethane) was maintained at 35 g_{cat} h mol_{ethane}^{-1}. A blank experiment carried out at 550 °C confirmed the absence of ethane conversion.

In a first set of experiments, the reactor was loaded with fresh catalyst and the ODH-C_2 reaction was performed at 440, 480, 500, or 550 °C. An independent experiment was performed at each temperature. When each of these tests was over, the reactor was cooled and the corresponding sample of spent catalyst was recovered. A second set of experiments was carried out to compare the catalytic performance of the fresh catalyst (MoVTeNbO-F) with that of a sample of spent catalyst. The material recovered from an experiment carried out under the most severe temperature conditions (550 °C), denoted as MoVTeNbO-S550, was chosen for this testing. Thus, two independent ODH-C_2 experiments, one over each of these two samples, were performed at reaction temperatures ranging from 440 to 550 °C for a contact time of 35 g_{cat} h mol_{ethane}^{-1}.

The ethane conversion and ethylene selectivity were defined on a carbon basis. The ethane conversion ($X_{C,ethane}$) was calculated using eq 1:

$$X_{C,ethane} = \frac{G^{\circ}_{C,ethane} - G_{C,ethane}}{G^{\circ}_{C,ethane}} \times 100\% \quad (1)$$

where $G^{\circ}_{C,ethane}$ and $G_{C,ethane}$ indicate the mass flow rates of ethane at the inlet and outlet of the reactor, respectively.

The selectivities for ethylene and oxidation products (CO and CO_2) were calculated on the basis of the carbon mass in component i formed per unit mass of carbon in ethane converted according to eq 2:

$$S_{C,i} = \frac{G_{C,i}}{G^{\circ}_{C,ethane} - G_{C,ethane}} \times 100\% \quad (2)$$

The ethane flow rate was measured under standard conditions [i.e., 1 atm (101.32 kPa) and 20 °C]. The molar flow rate of species i at the reactor outlet (F_i) was quantified indirectly via the internal standard method according to eq 3:

$$F_i = \frac{F^{\circ}_{N_2} M_{N_2}}{A_{N_2} CF_{N_2}} \times \frac{A_i CF_i}{M_i} \quad (3)$$

where M_i, A_i, and CF_i are the molecular mass, GC-integrated area, and GC calibration factor for product i; M_{N_2}, A_{N_2}, and CF_{N_2} are the corresponding values for nitrogen, which was used as the internal standard; and $F^{\circ}_{N_2}$ is the molar flow rate of N_2.

2.3. Characterization Techniques. *2.3.1. X-ray Diffraction.* The powder X-ray diffraction (XRD) patterns of pristine and spent catalysts were recorded on a Siemens D-500 diffractometer using a θ–θ configuration and a graphite-monochromatized secondary beam. Diffraction intensities were measured from 4 to 60° with a 2θ step of 0.02° for 8 s per point using Cu K$\alpha_{1,2}$ radiation with a wavelength of 1.5418 Å at 40 keV and 40 mA. The unit cell parameters of the M1, M2 and MoO_2 phases were refined by full pattern fitting with the MAUD program according to the Rietveld method using the M1 and M2 crystallographic information reported by DeSanto et al.[18] and Li et al.[19]

2.3.2. HRTEM and SEM. Samples were subjected to high-resolution transmission electron microscopy (HRTEM). Micrographs were obtained in a TITAN 80-300 microscope with a Schottky-type field-emission gun operating at 300 kV. The resolution point and information limit were better than 0.085 nm. HRTEM digital images were obtained using a CCD camera and DigitalMicrograph software from Gatan. Additionally, elemental composition was determined by energy-dispersive X-ray spectroscopy (EDS) with an EDAX spectrometer fitted to the transmission electron microscope. In order to prepare the materials for analysis, samples in powder form were ultrasonically dispersed in ethanol and then supported on holey carbon-coated copper grids.

The morphologies and elemental compositions of the catalysts were obtained by scanning electron microscopy (SEM). Images of samples were taken in a Nova-200 dual-beam microscope equipped with a Schottky-type field-emission gun using a resolution of 1.1 nm. An X-ray Si (Li) ultrathin window EDS spectrometer from EDAX was coupled for detection of elements from beryllium onward.

2.3.3. Raman Spectroscopy. The Raman spectra were recorded using a HORIBA Jobin Yvon T64000 spectrometer equipped with a confocal microscope (Olympus BX41) and an Ar^+ laser operating at 514.5 nm at a power of 10 mW. The spectrometer was equipped with a CCD camera detector.

The samples were excited by the 514.5 nm line of the Ar^+ laser (Spectra Physics model 171) with a laser power of 2.5 mW. The following spectrometer characteristics were used: microscope objective, 50×; spectral resolution, 2.5 cm^{-1}; integration time, 20 s per spectrum; number of scans, 50. Raman spectra were obtained at different points in each sample to determine the homogeneity and/or heterogeneity of the sample. The spatial resolution of each analysis was about 0.4 μm.

3. RESULTS AND DISCUSSION

3.1. Catalytic Testing. *3.1.1. Performance of the Pristine Catalyst.* Under the employed reaction conditions, ethylene, CO, and CO_2 were the only reaction products detected in the reactor effluent during ODH-C_2. The contributions of these products to the reactor effluent composition in fact evolved in the following order: ethylene ≫ CO > CO_2. However, the relative amounts of these compounds depend upon the specific reaction conditions (e.g., reaction temperature, space-time, etc.). Increasing the temperature or/and space time augmented the relative importance of the total oxidation products to the detriment of ethylene; this was more evidently observed in the case of temperature.

Figure 1 shows the ethane conversion and ethylene selectivity as a function of time on stream during ODH-C_2 over the MoVTeNb-F catalyst. These results suggest that the catalyst exhibited remarkable stability under the studied operating conditions (i.e. 440 °C and $C_2/O_2/N_2$ inlet molar ratio of 9/7/84). No significant changes in conversion or selectivity were detected during the repetition of three run tests with 7 h of time on stream, each using the same catalytic material (Figure 1). Notably, the catalyst exhibited ethane conversions of ca. 45% and 64% for contact times (W/F) of 35 and 70 g_{cat} h mol_{ethane}^{-1}, respectively. In addition, the selectivity for ethylene was remarkably high, reaching values of ca. 89–93%. The good stability in the catalytic performance of the

dx.doi.org/10.1021/cs500143j | ACS Catal. 2014, 4, 1292–1301

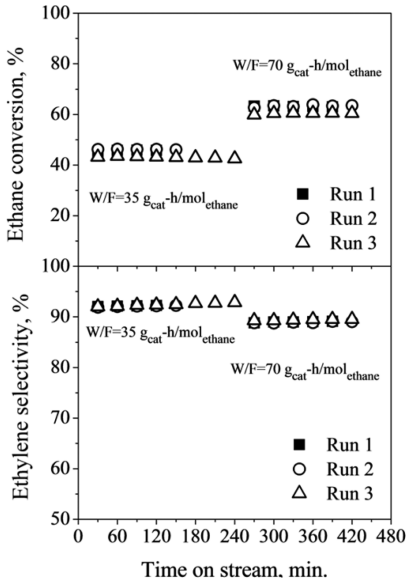

Figure 1. Ethane conversion and ethylene selectivity as functions of time on stream for three repeated ODH-C_2 reaction tests. Experiments were performed at 440 °C with a space time of 35 or 70 g_{cat} h mol_{ethane}^{-1} and a reactor inlet $C_2/O_2/N_2$ molar ratio of 9/7/84. Symbols: (■) run 1; (○) run 2; (△) run 3.

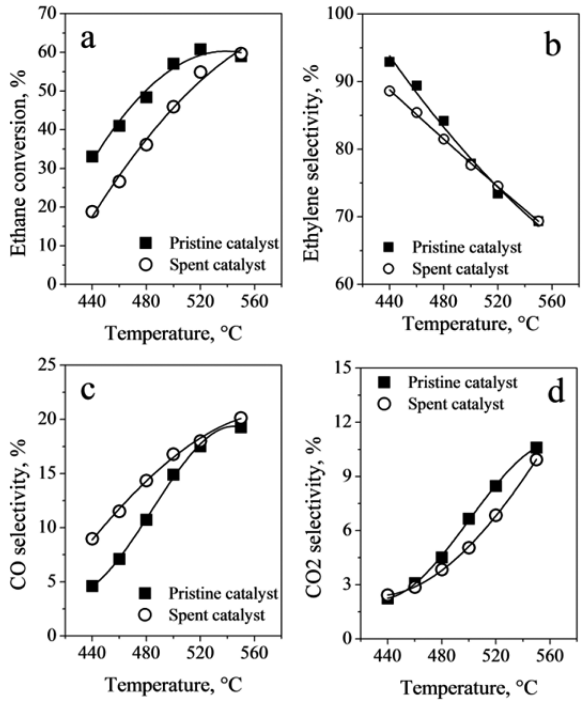

Figure 2. Plots showing steady-state data for (a) ethane conversion, (b) ethylene selectivity, (c) CO selectivity, and (d) CO_2 selectivity as functions of the reaction temperature. Experiments were performed over the MoVTeNb-F (■) and MoVTeNb-S550 (○) catalysts at a space time of 35 g_{cat} h mol_{ethane}^{-1} and a reactor inlet $C_2/O_2/N_2$ molar ratio of 9/7/84.

sample indicates that its active sites remain unchanged during the reaction tests at 440 °C.

3.1.2. Pristine Catalyst versus Spent Catalyst Performance. The exothermic character of both the main and side reactions during ODH-C_2 may lead to the formation of hot spots along the reactor bed. An uncontrolled increase in reactor temperature may damage the catalyst's crystalline structure irreversibly, altering the corresponding catalytic behavior. With the aim of assessing the thermal stability of the MoVTeNb mixed oxide, the catalytic performance of a pristine sample (MoVTeNb-F) was measured at a contact time (W/F) of 35 g_{cat} h mol_{ethane}^{-1} over the reaction temperature range from 440 to 550 °C. In addition, in order to evaluate the possible damage to the physicochemical properties in the spent samples, after catalytic tests at 440, 500, and 550 °C the samples were recovered and characterized. In addition, the deviations in the catalytic performance of the spent catalyst from the test at 550 °C (MoVTeNbO-S550) relative to the fresh catalyst (MoVTeNbO-F) were also quantified. To this end, two separate steady-state ODH-C_2 experiments were performed over each of these two samples in accordance with the protocol and reaction conditions outlined in section 2.2.

Figure 2 displays the variations in the ethane conversion and ethylene, CO, and CO_2 selectivities as functions of reaction temperature for the pristine and spent MoVTeNb mixed oxide catalysts. It can be observed in Figure 2a that from 440 to 520 °C both catalysts exhibited a linear increase in the ethane conversion. In the case of the pristine sample, augmenting the reaction temperature from 520 to 550 °C did not lead to an increase in ethane conversion; in fact, a slight decrease in the ethane conversion from 61 to 59 mol % was observed. A small decrease in ethylene selectivity with a concomitant increase in CO_x selectivity was also detected. This unexpected behavior might be related to catalyst damage caused by the high reaction temperature (520 °C) used in the preceding reaction stage.

In regard to the product distribution, Figure 2b–d shows that both the pristine and spent catalysts exhibited a monotonic increase in the selectivity for combustion products (CO and CO_2) with temperature to the detriment of ethylene. At the end of the test, when the catalyst was removed from the reactor, a silver-colored solid deposit was visually detected on its outlet connecting tube, particularly when reaction was conducted above 480 °C. Because of the temperature profile in the furnace that heats the reactor, the temperature at the reactor outlet is significantly lower than the one in the catalyst bed zone, which allowed this deposit to be observed.

In relation to the pristine catalyst, the spent catalyst was appreciably less active for ethane conversion, in particular when reaction was performed far below 520 °C. In relative terms, the spent catalyst was ca. 41% less active for ethane conversion than the pristine one in a comparison of the catalytic results at 440 °C. In regard to the selectivities for reaction products, however, the differences are fairly less evident than those found for ethane conversion and actually are detectable only at temperatures below 480 °C. In fact, at 440 °C, the temperature at which the maximum ethane conversion deviation was detected, the spent catalyst was around 4 percentage points less selective for ethylene compared with the pristine catalyst, while the CO_2 selectivity was slightly reduced, as observed in Figure 2d. From these results, it is inferred that the loss of ethane conversion in the spent catalyst should essentially be associated with a decrease in the density of active sites.

3.2. Analyses of Pristine and Spent Catalysts. In order to investigate the changes in the MoVTeNb catalyst after reactions at temperatures as high as 550 °C, the physicochemical properties of the pristine catalyst were compared with the corresponding ones for a series of spent catalysts.

3.2.1. X-ray Diffraction. The XRD patterns of MoVTeNb mixed oxide catalysts in the pristine and spent forms, the latter

dx.doi.org/10.1021/cs500143j | ACS Catal. 2014, 4, 1292–1301

after subjection to catalytic tests at 440, 500, and 550 °C, are compared in Figure 3. The experimental XRD patterns and the

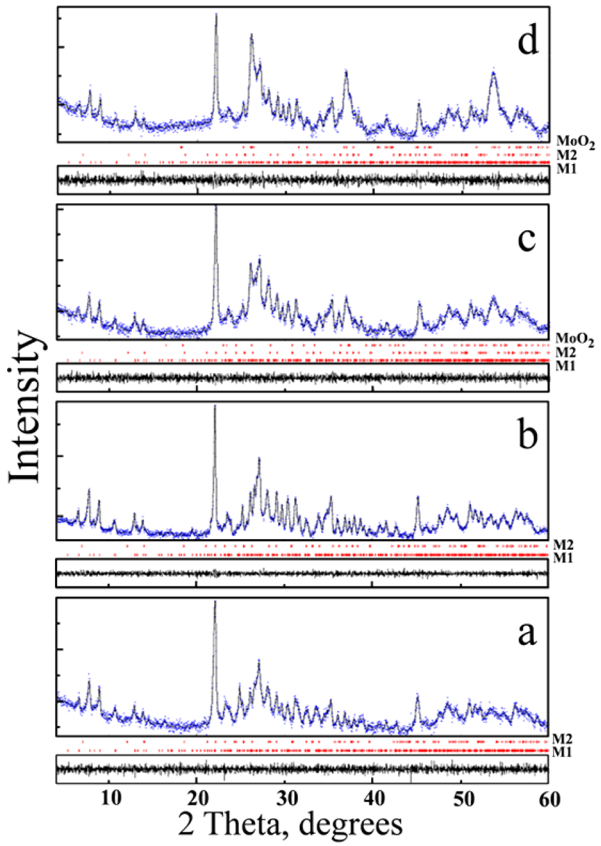

Figure 3. XRD patterns of the (a) MoVTeNb-F, (b) MoVTeNb-S440, (c) MoVTeNb-S500, and (d) MoVTeNb-S550 catalyst samples. The XRD patterns were refined using the Rietveld method.

simulated patterns obtained using the Rietveld method are included in this figure. The calculated distributions of phases (wt %) are shown in Table 1. Diffraction lines located at 2θ = 6.6, 7.7, 8.9, 22.1, and 27.1° corresponding to the orthorhombic $Te_2M_{20}O_{57}$ (M = Mo, V, Nb) M1 phase and those at 2θ = 22.1 and 28.1° associated with the orthorhombic distorted HTB-type $Te_{0.33}MO_{3.33}$ (M = Mo, V, Nb) M2 phase were detected in the MoVNbTe-F pattern (Figure 3a).[18,19,26,35] The MoVNbTe mixed oxide, commonly known as a mixture of M1 and M2 phases, is a composite in which the referred M1 crystalline structure has been proposed to be critical for optimal selectivity during partial oxidation or ammoxidation of propane[29−33] and ODH-C_2 conversion.[9−16] As reported in Table 1, M1 is the major crystalline phase present in this catalyst (95 wt % M1 vs only 5 wt % M2 crystalline phase). M1 has an orthorhombic polyhedral-network-type molybdenum bronze structure with a framework similar to those of Mo_5O_{14} and $Mo_{17}O_{47}$.[19] This phase can be also described with the generic formula $(TeO)_{1-x}(Mo,V,Nb)_{10}O_{28}$, wherein the TeO component is intercalated into framework channels. By analogy with the generic description of the M1 formula, the formula for M2 can be written as $(TeO)_{2-x}(Mo,V,Nb)_6O_{18}$.

Table 1. Distributions of Crystal Phases in the Pristine and Spent MoVTeNb Catalysts, Calculated Using the Rietveld Method

	crystalline phase (wt %)		
sample	M1	M2	MoO_2
MoVTeNb-F	95	5	0
MoVTeNb-S440	95	5	0
MoVTeNb-S500	86	4	10
MoVTeNb-S550	68	8	24

On the other hand, Figure 3b shows the XRD pattern of MoVTeNb-S440, a spent mixed oxide subjected to reaction at 440 °C. This sample shows an XRD pattern very similar to that exhibited by the corresponding pristine sample. Moreover, Rietveld refinement showed the same M1 and M2 crystalline phase composition. Therefore, under the particular reaction conditions studied, the MoVNbTe-S440 spent mixed oxide did not exhibit any detectable change in its crystalline structure, which is in agreement with the catalytic behavior reported in Figure 1. However, when the XRD pattern of the pristine catalyst is compared with that of the catalysts after catalytic testing at 500 °C (sample MoVTeNb-S500; Figure 3c) and 550 °C (sample MoVTeNb-S550; Figure 3d), differences are evident. From the XRD patterns it can be observed that increasing the reaction temperature to values of 500 °C or higher leads to changes in the crystalline structure of the pristine solid. From the XRD point of view, after catalytic testing at 500 °C (Figure 3c), the formation of monoclinic MoO_2 phase (ICDD 04-007-2356) is observed, apart from the presence of the M1 and M2 phases. On the basis of the relative intensities of the reflection lines of the monoclinic MoO_2 phase in Figure 3c,d, it is clear that increasing the reaction temperature up to 550 °C results in a more severe degradation of the structure of the MoVTeNb mixed oxide. After the ODH-C_2 reaction at 500 °C, the MoVTeNb mixed oxide contained 10 wt % MoO_2, which reached 24 wt % in MoVTeNb-S550. On the basis of the distributions of phases in Table 1, it is evident that the formation of the MoO_2 crystalline phase in the MoVTeNb-S550 sample mainly comes from destruction of the M1 crystalline phase.

3.2.2. HRTEM and SEM Analyses of Pristine and Spent Catalysts. The SEM image of the pristine sample (Figure 4a)

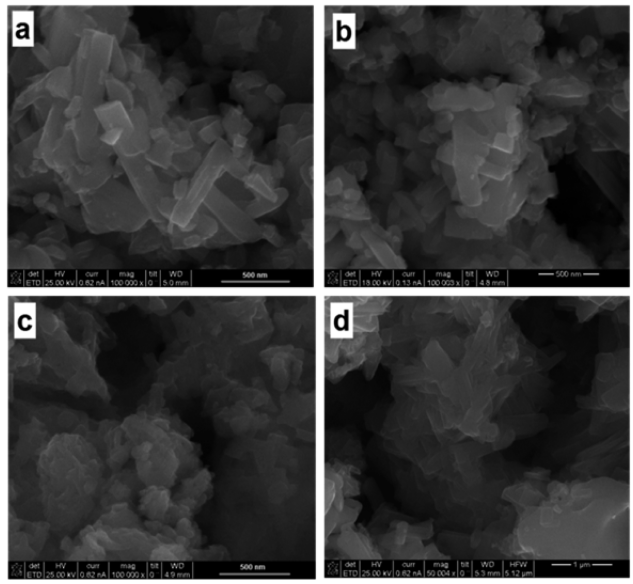

Figure 4. SEM micrographs of the (a) MoVTeNb-F, (b) MoVTeNb-S440, (c) MoVTeNb-S500 and (d) MoVTeNb-S550 catalyst samples.

dx.doi.org/10.1021/cs500143j | ACS Catal. 2014, 4, 1292−1301

shows the typical morphologies of the M1 phase (i.e., agglomeration of rodlike particles) and the M2 phase (i.e., platelet-like particles).[26,29,36] The morphology of the spent catalyst tested at 440 °C (Figure 4b) is rather similar to that of the pristine catalyst, which is consistent with what was observed in the XRD analysis. The spent catalyst resulting from the test performed at 500 °C, however, shows a different morphology (Figure 4c) compared with the pristine catalyst and the spent catalyst tested at 440 °C. In particular, it can be observed in the MoVTeNbO-S500 sample that the proportion of needlelike M1 phase agglomeration decreases, and sintering of the sample is noted. Apparently, atoms from this sample diffuse across the boundaries of the particles, fusing the particles together and creating solid agglomerates. Such a phenomenon is even more pronounced in the spent sample tested at 550 °C (Figure 4d), corresponding to the behavior also observed through the XRD analysis (Figure 3), wherein a rise of diffraction peaks corresponding to MoO_2 phase was detected.

The HRTEM image of the pristine catalyst (Figure 5a) shows well-defined rodlike particles together with others having

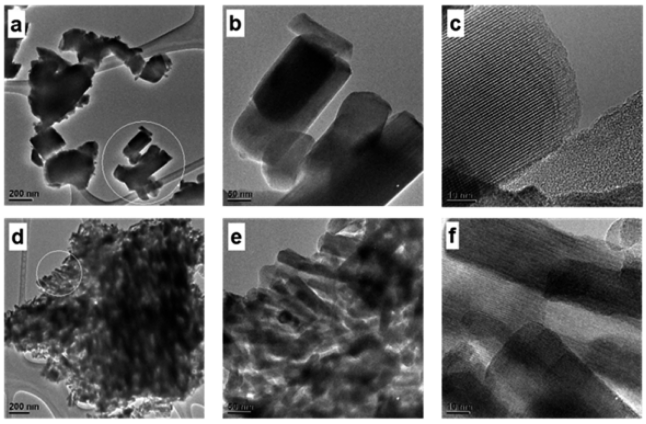

Figure 5. HRTEM micrographs at several magnifications for (a–c) the pristine sample MoVTeNb-F and (d–f) the spent catalyst after reaction at 550 °C, MoVTeNb-S550.

an irregular morphology. A higher magnification of the selected zone shows more clearly the rodlike particles and the crystallinity of the solid (Figure 5b,c). In contrast, the sample evaluated at 550 °C exhibits a different morphology with more irregular particles compared with the pristine sample, as can be observed in Figure 5d. In fact, the MoVTeNbO-S550 sample is composed of longer and thinner particles, which are easily identified in the image in Figure 5e. Additionally, a certain loss of crystallinity along with segregation/separation of the rodlike particles is noted, as illustrated in Figure 5f.

In order to study the loss of crystallinity in the spent catalyst tested at 550 °C (i.e., MoVTeNb-550), EDS and HRTEM were performed on crystals with rodlike morphology (Figure 6). This kind of morphology indicates the presence of the M1 phase. Table 2 contains information from the EDS chemical analyses, which were carried out at the center and at the ends of a long crystal. The areas of the crystal where the elemental analyses were performed are circled. From data in Table 2, it is noteworthy that the chemical composition across the crystal is not homogeneous. The chemical composition measured at the center of the crystal (i.e., $MoV_{0.15}Te_{0.09}Nb_{0.19}$) is not far from that obtained by atomic absorption spectroscopy (i.e., $MoV_{0.25}Te_{0.11}Nb_{0.16}$), whereas that measured at the ends of

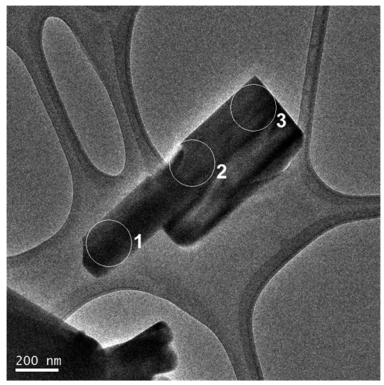

Figure 6. HRTEM micrograph of an M1 crystal of the spent catalyst after ODH-C_2 reaction at 550 °C (MoVTeNb-S550). Circles indicate the zones where EDS chemical analyses were carried out (i.e., EDS-1, EDS-2, and EDS-3 in Table 2).

Table 2. Chemical Compositions of MoVTeNb-S550 Obtained from EDS Analyses[a]

element(s)	EDS-1	EDS-2	EDS-3
	composition (atom %)		
O	67	30	70
V	4	7	4
Nb	3	10	2
Mo	25	49	23
Te	0.8	4	1
	atom ratios		
V/Mo	0.16	0.14	0.17
Te/Mo	0.03	0.08	0.04
Nb/Mo	0.12	0.20	0.09

[a]EDS-1, EDS-2, and EDS-3 correspond to circled zones 1, 2, and 3, respectively, in Figure 6.

the crystal presents lower contents of Te and Nb compared with the central part of the crystal. Actually, the chemical compositions at the two ends of the crystal are essentially the same (i.e., $MoV_{0.16}Te_{0.035}Nb_{0.10}$) and indicate a loss of around 68 wt % Te and 37.5 wt % Nb compared with the values at the center of the crystal. Thus, it is likely that under a reducing atmosphere at a high temperature (≥500 °C) in the catalytic zone, Te reduction occurs preferentially across the [001] zone axis of the M1 phase. This seems to be associated with a higher reactivity of this plane, as suggested in the literature.[17,18,20,21] On the other hand, HRTEM images were obtained for the same catalyst at the ends of several crystals with rodlike morphology (M1 phase). Figure 7a shows an HRTEM image of crystalline material exhibiting damage associated with Te removal, and its corresponding selected-area electron diffraction (SAED) pattern is presented in Figure 7b. Surprisingly, contrary to the typical series of spots, the SAED pattern appears as a series of small concentric lines. Actually, these elongated spots are composed of sets of spots. This remarkable finding suggests that this kind of SAED pattern shows the decomposition of the M1 phase, and probably the M2 phase, into the MoO_2 phase, as established by the XRD analysis of this sample. The profile shown in the Figure 7b inset confirms that the elongated spot is composed of a set of spots. The innermost spot, with an interplanar atomic distance of 4.03 Å, could correspond to either the M1 or M2 phase, while the last spot at 3.3 Å indicates the presence of atomic planes associated with the MoO_2 phase, the latter also observed by XRD. The

dx.doi.org/10.1021/cs500143j | ACS Catal. 2014, 4, 1292–1301

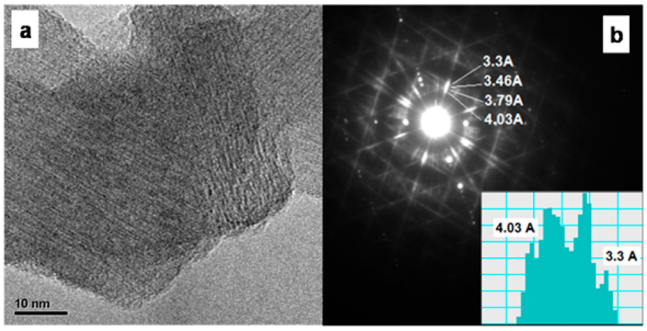

Figure 7. (a) HRTEM micrograph and (b) SAED pattern of a particle of spent catalyst after reaction at 550 °C (MoVTeNb-S550).

interpretation of this SAED pattern allows us to state that a fraction coming mainly from the original M1 phase decomposes to other phases by contraction of the original crystal while keeping the same habitat and orientation, comparable to an epitaxial growth, and together with the original phases causes the elongated spots. As evidenced by the XRD study, the extra phases correspond to MoO_2 but probably also to MoO_3, Mo_5O_{14}, $(Mo_{0.93}V_{0.07})_5O_{14}$ and $Mo_{0.97}V_{0.95}O_5$ phases, which are present in small amounts in the spent sample and therefore were not clearly detected by XRD.

Furthermore, in order to track the migration of tellurium in the pristine catalyst and the spent catalyst tested at 550 °C, chemical analyses by EDS in different regions of the samples were carried out. The results indicated that no segregated Te particles were found, in concordance with the XRD results.

3.2.3. HRTEM and EDS Analyses of the Solid Detached from the Catalyst. The silver-colored deposit formed at the reactor outlet after the catalytic tests at higher temperatures was recovered and then analyzed by HRTEM and EDS. Figure 8a displays a typical low-magnification image of this material, in which particles with sharp needle morphology can be observed. The lattice fringe of parallel planes observed in the high-magnification image (Figure 8b) was identified as metallic tellurium. EDS analysis of such particles confirmed that these sharp-needle particles are constituted by metallic tellurium. They essentially consist of 98 wt % Te, with the other 2 wt % corresponding to V and O (Figure 8c). The loss of Te might be related to the combination of a reducing atmosphere and a high reaction temperature (>500 °C) in the reactor zone. The loss of Te during the MoVTeNbO mixed oxide heat-treatment step has been explained by presence of oxalate ions in the Nb source, which would progressively reduce the Te^{4+} to Te; the metallic Te would then be detached from the solid by melting.[34] In the present study, the loss of tellurium during the ODH-C_2 reaction at high temperature (>500 °C) can be also associated with a reduction reaction.[37] The presence of ethane and nitrogen in the mixture feed, in combination with a high temperature, favor the gradual reduction of Te from Te^{4+} to Te^0. Metallic Te has a melting point of ca. 450 °C, and its vapor pressure strongly depends on the pressure and temperature of the system.[38,39] Indeed, the pressure of the system was not varied, only the reaction temperature. Thus, when reaction temperature was higher than 500 °C and part of the Te^{4+} (that in the most accessible zones) was reduced to Te^0, it melted, and the liquid Te then vaporized, trying to reach its equilibrium vapor pressure. However, the continuous flow of products and reactants along the catalytic bed is sufficient for tellurium vapor to be entrained out of the reactor. The heated

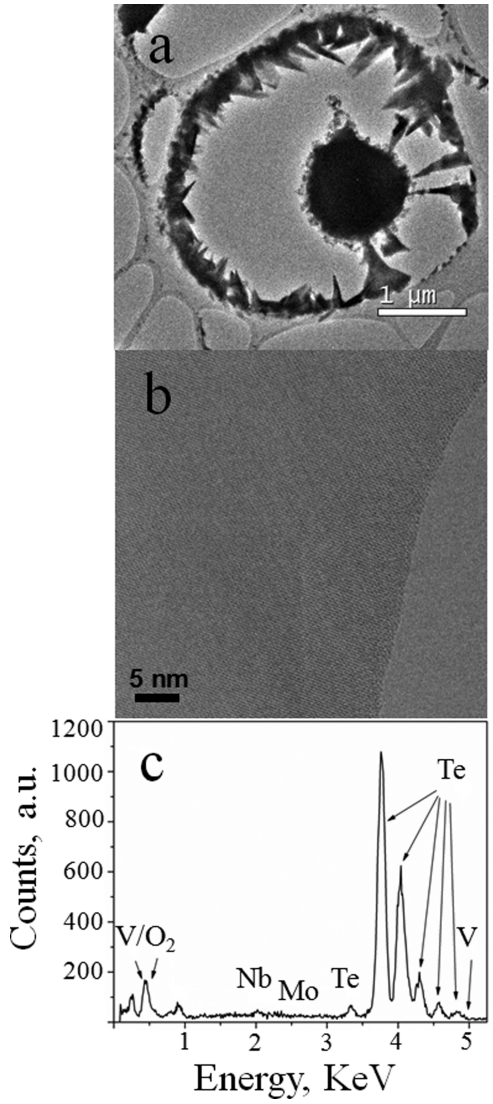

Figure 8. Characterization of the material recovered from the reactor outlet after the catalytic testing at 550 °C: (a, b) bright-field HRTEM images; (c) chemical composition analysis of needlelike particles by the EDS technique.

zone avoids Te^0 condensation, causing it to be deposited at the cold reactor exit. As observed by XRD, the removal of tellurium from the intercalated framework channels of the M1 phase brings about the partial destruction of the MoVTeNbO mixed oxide with the simultaneous formation of the MoO_2 phase. The loss of long-range order in the low-angle peaks ($5° \leq 2\theta \leq 10°$), related to the superstructure of the M1 phase, also evidences the detachment of Te from the M1 superstructure, although some detachment of Te from the M2 phase cannot be discarded.

It must be noticed that the MoVTeNbO-F sample was a mixed oxide that was chemically and structurally stabilized via a thermal treatment procedure. This material was actually heat-treated under a flow of nitrogen at 600 °C for 2 h. As explained above, an important loss of tellurium from this activated sample in the form of metallic tellurium during such a thermal treatment has been reported.[34] Although this second loss of Te from the highly active and selective MoVTeNb mixed oxide catalyst during the ODH-C_2 reaction was observed only at high temperatures (≥500 °C), it is an important point to consider in

dx.doi.org/10.1021/cs500143j | ACS Catal. 2014, 4, 1292−1301

the scale-up of the ODH-C_2 process. The high exothermicity of this reaction, and mainly those of secondary CO_x reactions, can facilitate the formation of hot points that could irreversibly damage the catalyst. The removal of Te from the catalyst not only decreases the Te/(Mo + V + Nb) ratio but also modifies the crystal phase composition. Accordingly, the nature of the crystalline phases and the catalytic performance of the heat-treated materials strongly depends on the final chemical composition of the catalysts.

As a general trend, the ethane conversion decreased, without a significant loss of ethylene selectivity, as the loss of tellurium was enhanced with concomitant MoO_2 formation. This means that (1) Te has an important role in both the stabilization of the M1 crystalline phase and the formation of active sites and (2) the MoO_2 crystalline phase is a spectator in the ODH-C_2 reaction.

At this point, although Ueda et al.[40] have shown that it is possible to obtain the M1 phase by hydrothermal synthesis without tellurium (Mo−V-based catalyst), it has been established that Te^{4+} plays an important role in the stabilization of the hexagonal channels of this phase.[29,41−46] Thus, the role of Te in the most active and selective catalysts should be directly associated not with ethane activation but instead with the formation of an active and selective crystalline phase, $Te_2M_{20}O_{57}$,[47] for the oxidative activation of both ethane and propane and, additionally, for the elimination of nonselective Mo-containing crystalline phases, especially MoO_2 and/or other MoVNbO-related compounds generally proposed in Te-free MoVNbO mixed oxide catalysts.[25,48−53]

3.2.4. Raman Spectroscopy. The Raman spectra of pristine and spent catalysts are shown in Figure 9. Since the XRD pattern of the MoVTeNbO-S440 spent catalyst was very similar to that of pristine sample, only the Raman spectra of spent samples catalytically tested at 500 and 550 °C are presented. The Raman spectrum of the pristine sample (Figure 9a) presents an intense band at 870 cm^{-1} with a broad shoulder toward lower frequency centered at about 820 cm^{-1} and a weak shoulder toward higher frequency at around 970 cm^{-1}. Two other Raman bands at lower frequencies (450 and 466 cm^{-1}), hardly resolved, are also observed. The profile of this spectrum is similar to those previously reported for these types of mixed oxide materials.[54] The shoulder at 970 cm^{-1} can be assigned to stretching vibrations of terminal Mo═O and V═O bonds,[55] whereas the bands appearing in the 770−880 cm^{-1} range have been associated with asymmetric M−O−M bridge stretching modes. The low-frequency bands at around 470 cm^{-1} appear in a typical regime of the symmetric M−O−M bridge stretching modes. López Nieto and co-workers[13] showed that an intense Raman band at 874 cm^{-1} is present on both pure M1 and M2 phases, whereas M−O−M stretching modes are observed in both M1 and M2 crystalline phases. They assigned bands located at 796 and 437 cm^{-1} to the M2 phase, which are shifted to higher frequencies (827 and 470 cm^{-1}) in the case of the M1 phase. Consequently as expected, the Raman spectra of the pristine catalyst allowed the presence of the M1 and M2 crystalline phases to be identified, in agreement with the XRD results.

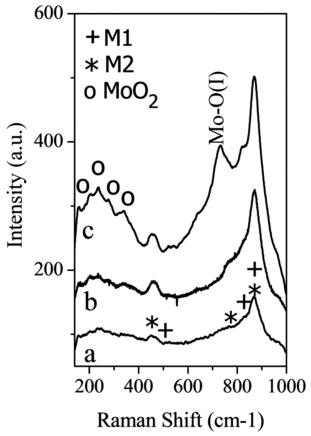

Figure 9. Raman spectra of (a) pristine catalyst (MoVTeNb-F) and (b, c) spent catalysts after ODH-C_2 reaction at (b) 500 °C (MoVTeNb-S500) and (c) 550 °C (MoVTeNb-S550).

The comparison between the pristine sample and the spent catalyst designated as MoVNbO-S550 on the basis of corresponding Raman spectra indicates significant differences, especially in the low-frequency Raman region. The Raman spectrum of MoVNbO-S550 (Figure 9c) presents clearly identified bands in the low-frequency region at 203, 228, 280, and 340 cm^{-1} that are associated with the MoO_2 crystalline phase. A more intense band toward higher frequencies located at 732 cm^{-1} is also observed. It should be noted that all of these bands are more clearly detected in the spent catalyst MoVNbO-S500 (Figure 9b) while in the case of the pristine catalyst they are practically not visible (Figure 9a). Dieterle and Mestl[56] reported Raman bands of reduced monoclinic MoO_2 at 207, 230, 347, 364, 458, 496, 569, 585, and 740 cm^{-1}. The same assignation of bands was also reported by Bolzan et al.[57] The Raman bands at 744 and 589 cm^{-1} have been attributed to the stretching vibrations of the Mo−O(I) and Mo−O(II) groups in the MoO_2 lattice. Thus, the Raman bands at 203, 228, 280, 340, and 732 cm^{-1} that can clearly be observed for the MoVTeNbO-550S spent catalyst are associated with the monoclinic MoO_2 phase that was segregated from the M1 and M2 phases by the effect of Te detachment from the intercalated framework channels of the M1 and M2 phases under the reaction conditions. The broad band at 458 cm^{-1} comes from overlap of the 458 cm^{-1} MoO_2 Raman band and the Raman bands of the M2 and M1 phases centered at 450 and 466 cm^{-1}, respectively. In the MoVTeNbO-S550 spent catalyst, the Mo−O(II) stretching vibration of the MoO_2 lattice was not observed, and the stretching vibration of the Mo−O(I) groups is shifted by 12 cm^{-1} toward lower frequency. This may be explained in terms of the strong interactions between the different reduced molybdenum oxide species being formed from the progressive destruction of the M1 and M2 phases, as suggested by HRTEM.

4. CONCLUSIONS

The MoVTeNb mixed oxide is a highly active and selective catalyst for ODH-C_2 to give ethylene that shows remarkable stability when it operates at temperatures lower than 500 °C. The catalyst exhibited a conversion about of 50% with an ethylene selectivity higher than 90% at $T_{reaction}$ = 440 °C and a contact time of 35 g_{cat} h mol_{ethane}^{-1}. Nevertheless the catalyst's stability is restricted to operation below 500 °C, mostly due to a combination of reaction temperature and feed composition (in this case, the inlet $C_2/O_2/N_2$ molar ratio was 9/7/84). This result was unexpected since the catalyst was previously activated by calcination at 600 °C under a flow of N_2, where an important amount of Te was lost. Operation above 500 °C brings about the removal of tellurium from the MoVTeNb

dx.doi.org/10.1021/cs500143j | ACS Catal. 2014, 4, 1292−1301

mixed oxide catalysts; the loss of tellurium occurs preferentially from the end section of the M1 crystal phase, across the [001] plane. Removal of tellurium from the intercalated framework channels of the M1 phase leads to partial destruction of the MoVTeNb mixed oxide, chiefly generating a MoO_2 crystalline phase and in consequence decreasing the catalyst's activity. The preservation of ethylene selectivity after loss of Te indicates that the catalytic sites remain unchanged and that only a loss of them happens. Also, no direct effect of the MoO_2 crystalline phase over the ODH-C_2 reaction was observed except for the decreased conversion due to destruction of the M1 crystalline phase. The detachment of tellurium from the MoVTeNb mixed oxide catalysts is carried out by means of a reduction process of Te^{4+} to Te^0. Thus, hot spots along the reactor bed should be avoided or controlled in order to keep the catalytic bed temperature below 500 °C.

AUTHOR INFORMATION

Corresponding Authors

*E-mail: jsanchez@imp.mx.

*E-mail: harmenda@imp.mx.

Notes

The authors declare no competing financial interest.

ACKNOWLEDGMENTS

This work was financially supported by the Instituto Mexicano del Petróleo.

REFERENCES

(1) Lippe, D. *Oil Gas J.* **2011**, *109*, 94−99.

(2) Bhasin, M. M. *Top. Catal.* **2003**, *23*, 145−149.

(3) Sanfilipp, D.; Miracca, I. *Catal. Today* **2006**, *111*, 133−139.

(4) Grabowski, R. *Catal. Rev.: Sci. Eng.* **2006**, *48*, 199−268.

(5) Cavani, F.; Ballarini, N.; Cercola, A. *Catal. Today* **2007**, *127*, 113−131.

(6) Bhasin, M. M.; McCain, J. H.; Vora, B. V.; Imai, T.; Pujado, P. R. *Appl. Catal., A* **2001**, *221*, 397−419.

(7) Gärtner, C. A.; van Veen, A. C.; Lercher, J. A. *ChemCatChem* **2013**, *5*, 3196−3217.

(8) Lange, J. P.; Schoonebeek, R. J.; Mercera, P. D. L.; van Breukelen, F. W. *Appl. Catal., A* **2005**, *283*, 243−253.

(9) Valente, J. S.; Quintana-Solórzano, R.; Armendáriz-Herrera, H.; Barragán-Rodríguez, G.; López Nieto, J. M. *Ind. Eng. Chem. Res.* **2014**, *53*, 1775−1786.

(10) Lopez Nieto, J. M.; Botella, P.; Vázquez, M. I.; Dejoz, A. *Chem. Commun.* **2002**, 1906−1907.

(11) Lopez Nieto, J. M.; Botella, P.; Vázquez, M. I.; Dejoz, A. WO 03/064035 A1, 2003; assigned to CSIC-UPV.

(12) Lopez Nieto, J. M.; Botella, P.; Vázquez, M. I.; Dejoz, A. U.S. Patent 7,319,179 B2, 2008; assigned to CSIC-UPV.

(13) Solsona, B.; Vázquez, M. I.; Ivars, F.; Dejoz, A.; Concepción, P.; Lopez Nieto, J. M. *J. Catal.* **2007**, *252*, 271−280.

(14) Nguyen, T. T.; Burel, L.; Nguyen, D. L.; Pham-Huu, C.; Millet, J. M. M. *Appl. Catal., A* **2012**, *433*, 41−48.

(15) Xie, Q.; Chen, L.; Weng, W.; Wan, H. *J. Mol. Catal. A: Chem.* **2005**, *240*, 191−196.

(16) Nguyen, T. T.; Aouine, M.; Millet, J. M. M. *Catal. Commun.* **2012**, *21*, 22−26.

(17) Aouine, M.; Dubois, J. L.; Millet, J. M. M. *Chem. Commun.* **2001**, 1180−1181.

(18) DeSanto, P.; Buttrey, D. J.; Grasselli, R. K.; Lugmair, C. G.; Volpe, A. F.; Toby, B. H. *Top. Catal.* **2003**, *23*, 23−38.

(19) Li, X.; Buttrey, D. J.; Blom, D. A.; Vogt, T. *Top. Catal.* **2011**, *54*, 614−626.

(20) Deniau, B.; Millet, J. M. M.; Loridanta, S.; Christin, N.; Dubois, J. L. *J. Catal.* **2008**, *260*, 30−36.

(21) Botella, P.; García-González, E.; Lopez Nieto, J. M.; González-Calbet, J. M. *Solid State Sci.* **2005**, *7*, 507−519.

(22) Murayama, H.; Vitry, D.; Ueda, W.; Fuchs, G.; Anne, M.; Dubois, J. L. *Appl. Catal., A* **2007**, *318*, 137−142.

(23) Wagner, J. B.; Timpe, O.; Hamid, F. A.; Trunschke, A.; Wild, U.; Su, D. S.; Widi, R. K.; Hamid, S. B. A.; Schlögl, R. *Top. Catal.* **2006**, *38*, 51−58.

(24) Hävecker, M.; Wrabetz, S.; Kröhnert, J.; Csepei, L.-I.; Naumann d'Alnoncourt, R.; Kolenko, Y. V.; Girgsdies, F.; Schlögl, R.; Trunschke, A. *J. Catal.* **2012**, *285*, 48−60.

(25) López Nieto, J. M.; Botella, P.; Concepción, P.; Dejoz, A.; Vázquez, M. I. *Catal. Today* **2004**, *91−92*, 241−245.

(26) Garcia-González, E.; López Nieto, J. M.; Botella, P.; González-Calbet, J. M. *Chem. Mater.* **2002**, *14*, 4416−4421.

(27) Oliver, J. M.; López Nieto, J. M.; Botella, P.; Mifsud, A. *Appl. Catal., A* **2004**, *257*, 67−76.

(28) Solsona, B.; López Nieto, J. M.; Oliver, J. M.; Gumbau, J. P. *Catal. Today* **2004**, *91−92*, 247−250.

(29) Grasselli, R. K.; Burrington, J. D.; Buttrey, D. J.; DeSanto, P.; Lugmair, C. G.; Volpe, A. F.; Weingand, T. *Top. Catal.* **2003**, *23*, 5−22.

(30) Holmberg, J.; Grasselli, R. K.; Andersson, A. *Top. Catal.* **2003**, *23*, 55−63.

(31) Grasselli, R. K.; Buttrey, D. J.; Burrington, J. D.; Andersson, A.; Holmberg, J.; Ueda, W.; Kubo, J.; Lugmair, C. G.; Volpe, A. F. *Top. Catal.* **2006**, *38*, 7−16.

(32) Guliants, V. V.; Bhandari, R.; Swaminathan, B.; Vasudevan, V. K.; Brongersma, H. H.; Knoester, A.; Gaffney, A. M.; Han, S. *J. Phys. Chem. B* **2005**, *109*, 24046−24055.

(33) Grasselli, R. K.; Buttrey, D. J.; DeSanto, P.; Burrington, J. D.; Lugmair, C. G.; Volpe, A. F.; Weingand, T. *Catal. Today* **2004**, *91−92*, 251−258.

(34) Ivars, F.; Solsona, B.; Hernández, S.; López-Nieto, J. M. *Catal. Today* **2010**, *149*, 260−266.

(35) Millet, J. M. M.; Roussel, H.; Pigamo, A.; Dubois, J. L.; Jumas, J. C. *Appl. Catal., A* **2002**, *232*, 77−92.

(36) Tsuji, H.; Koyasu, Y. *J. Am. Chem. Soc.* **2002**, *124*, 5608−5609.

(37) Deniau, B.; Nguyen, T. T.; Delichere, P.; Safonova, O.; Millet, J.-M. M. *Top. Catal.* **2013**, *56*, 1952−1962.

(38) Machol, R. E.; Westrum, E. F., Jr. *J. Am. Chem. Soc.* **1958**, *80*, 2950−2952.

(39) Machol, R. E.; Westrum, E. F., Jr. *J. Phys. Chem.* **1958**, *62*, 361−362.

(40) Ueda, W.; Vitry, D.; Katou, T. *Catal. Today* **2005**, *99*, 43−49.

(41) Botella, P.; Solsona, B.; Martínez-Arias, A.; López-Nieto, J. M. *Catal. Lett.* **2001**, *74*, 149−154.

(42) Botella, P.; López Nieto, J. M.; Solsona, B.; Mifsud, A.; Márquez, F. *J. Catal.* **2002**, *209*, 445−455.

(43) Ueda, W.; Oshihara, K. *Appl. Catal., A* **2000**, *200*, 135−143.

(44) Watanabe, H.; Koyasu, Y. *Appl. Catal., A* **2000**, *194−195*, 479−485.

(45) Al-Saeedi, J. N.; Vasudevan, V. K. J.; Guliants, V. V. *Catal. Commun.* **2003**, *4*, 537−542.

(46) Botella, P.; Concepción, P.; López Nieto, J. M.; Moreno, Y. *Catal. Today* **2005**, *99*, 51−57.

(47) López Nieto, J. M.; Botella, P.; Solsona, B.; Oliver, J. M. *Catal. Today* **2003**, *81*, 87−94.

(48) Thorsteinson, E. M.; Wilson, T. P.; Young, F. G.; Kasai, P. H. *J. Catal.* **1978**, *52*, 116−132.

(49) Ruth, K.; Burch, R.; Kieffer, R. *J. Catal.* **1998**, *175*, 27−39.

(50) Mezourki, M.; Taouk, B.; Tessier, L.; Bordes, E.; Courtine, P. *Stud. Surf. Sci. Catal.* **1993**, *75*, 753−764.

(51) Botella, P.; López-Nieto, J. M.; Dejoz, A.; Vázquez, M. I.; Martínez-Arias, A. *Catal. Today* **2003**, *78*, 507−512.

(52) Ueda, W.; Oshihara, K.; Vitry, D.; Hisano, T.; Kayashima, Y. *Catal. Surv. Jpn.* **2002**, *6*, 33−44.

(53) McCain, J. H., U.S. Patent 4,524,236, 1985; assigned to Union Carbide Corp.

(54) Ushikubo, T.; Oshima, K.; Kayou, A.; Hatano, M. *Stud. Surf. Sci. Catal.* **1997**, *112*, 473−480.
(55) Wachs, I. E.; Jehng, J.-M.; Ueda, W. *J. Phys. Chem. B* **2005**, *109*, 2275−2284.
(56) Dieterle, M.; Mestl, G. *Phys. Chem. Chem. Phys.* **2002**, *4*, 822−826.
(57) Bolzan, A. A.; Kenned, B. J.; Howard, C. J. *Aust. J. Chem.* **1995**, *48*, 1473−1477.